Xu *et al. Energy Mater* 2024;4:400005
**DOI:** 10.20517/energymater.2023.73

**Energy Materials**

**Article**

**Open Access**

Check for updates

# Promoting the reversibility of electrolytic $MnO_2$-Zn battery with high areal capacity by $VOSO_4$ mediator

**Yong Xu, Wenjie Huang, Jun Liu, Renzong Hu, Liuzhang Ouyang, Lichun Yang*, Min Zhu**

School of Materials Science and Engineering, Guangdong Provincial Key Laboratory of Advanced Energy Storage Materials, South China University of Technology, Guangzhou 510640, Guangdong, China.

***Correspondence to:** Prof./Dr. Lichun Yang, School of Materials Science and Engineering, Guangdong Provincial Key Laboratory of Advanced Energy Storage Materials, South China University of Technology, 381 Wushan Road, Tianhe District, Guangzhou 510640, Guangdong, China. E-mail: mslcyang@scut.edu.cn

**How to cite this article:** Xu Y, Huang W, Liu J, Hu R, Ouyang L, Yang L, Zhu M. Promoting the reversibility of electrolytic $MnO_2$-Zn battery with high areal capacity by $VOSO_4$ mediator. *Energy Mater* 2024;4:400005. https://dx.doi.org/10.20517/energymater.2023.73

**Received:** 15 Sep 2023 **First Decision:** 8 Oct 2023 **Revised:** 25 Oct 2023 **Accepted:** 8 Nov 2023 **Published:** 5 Jan 2024

**Academic Editor:** Jiazhao Wang **Copy Editor:** Fangling Lan **Production Editor:** Fangling Lan

## Abstract

Electrolytic $MnO_2$-Zn batteries possess high energy density due to the high reduction potential and capacity of the cathode $Mn^{2+}/MnO_2$. However, the low reversibility of the $Mn^{2+}/MnO_2$ conversion results in a limited lifespan. In this study, we propose the utilization of $VOSO_4$ as a redox mediator in the $MnO_2$-Zn battery to facilitate the dissolution of $MnO_2$. Through various techniques such as electrochemical measurements, *ex-situ* UV-visible spectroscopy, X-ray diffraction, and scanning electron microscopes, we validate the interaction between $VO^{2+}$ and $MnO_2$, which effectively mitigates the accumulation of $MnO_2$. The introduction of the redox mediator results in exceptional redox reversibility and outstanding cycling stability of the $MnO_2/VOSO_4$-Zn battery at high areal capacities, with 900 cycles at 5 mAh $cm^{-2}$ and 500 cycles at 10 mAh $cm^{-2}$. Notably, even in the flow battery device, the battery exhibits a stable cycling performance over 300 cycles at 20 mAh $cm^{-2}$. These research findings shed light on the potential large-scale application of electrolytic $MnO_2$-Zn batteries.

**Keywords:** Electrolytic $MnO_2$-Zn batteries, high areal capacity, redox mediators, $VOSO_4$, cycling stability

## INTRODUCTION

Lithium-ion batteries have emerged as the leading power source due to their exceptional energy density[1,2]. However, the flammability and toxicity of organic electrolytes have raised significant safety concerns,

restricting their widespread use in energy storage applications[3,4]. In light of these challenges, aqueous zinc (Zn)-ion batteries have gained considerable attention. Zn, with its low reduction potential (-0.763 V *vs.* SHE) [Equation (1)], abundant reserves, and affordable price, stands out as an attractive option. Furthermore, the use of aqueous electrolytes ensures inherent safety and environmental friendliness[5-9].

In the realm of Zn-ion batteries, $MnO_2$ has traditionally served as a cathode material. It exhibits a theoretical capacity of 308 mAh $g^{-1}$ by allowing the intercalation of $Zn^{2+}$ and/or $H^+$ ions while reducing $Mn^{4+}$ to $Mn^{3+}$[10,11]. Recently, a novel electrolytic mechanism of $MnO_2$ [Equation (2)] has been reported. The two-electron transfer reaction involves the deposition and dissolution of $MnO_2$, resulting in an impressive theoretical capacity of 616 mAh $g^{-1}$[12-18]. Notably, the $MnO_2$-Zn battery benefits from the high reduction potential of $Mn^{2+}/MnO_2$ (1.228 V), enabling it to achieve a high voltage output of 1.991 V[19-28].

$$Zn^{2+} + 2e^- \rightarrow Zn \qquad E = -0.763 \text{ V } vs. \text{ SHE} \qquad (1)$$

$$Mn^{2+} + 2H_2O \rightarrow MnO_2 + 4H^+ + 2e^- \qquad E = 1.228 \text{ V } vs. \text{ SHE} \qquad (2)$$

However, electrolytic $MnO_2$-Zn batteries exhibit a limited cycling lifespan due to the incomplete dissolution of deposited $MnO_2$. This issue is exacerbated by the accumulation of $MnO_2$ particles, which can detach from the current collector and block ion transportation channels in the separator. Consequently, substantial polarization and rapid capacity degradation occur in the battery[29,30].

To address this prominent issue, various ions have been introduced into the electrolyte of electrolytic $MnO_2$-Zn batteries to enhance their electrochemical performance[31-36]. For instance, the incorporation of $Ni^{2+}$ ions serves as a catalyst for the $Mn^{2+}/MnO_2$ reaction kinetics, enabling charge and discharge at a rate of 50 C while maintaining a lifespan of over 450 cycles at an areal capacity of 1 mAh $cm^{-2}$[31]. Additionally, $Al^{3+}$ ions play a vital role in promoting $MnO_2$ dissolution by creating oxygen vacancies during deposition, leading to improved cycling stability over 2,000 cycles at an areal capacity of 2 mAh $cm^{-2}$[36]. Another approach involves the utilization of redox mediators such as $I^-$ and $Br^-$ ions[30,33], which interact with $MnO_2$ to prevent its accumulation. This mechanism has shown promising results, extending the lifespan of electrolytic $MnO_2$-Zn batteries to over 100 cycles at an areal capacity of 5 mAh $cm^{-2}$. Nevertheless, achieving enhanced reversibility and cyclic stability, particularly at high areal capacities, remains a significant challenge.

In this study, we employ $VOSO_4$ as a redox mediator to enhance the dissolution of $MnO_2$ in the electrolytic $MnO_2$-Zn battery. $VOSO_4$ is commonly utilized as an active component in the cathode of vanadium-based flow batteries due to its favorable reversibility and stability[37,38], Given that the reduction potential of the $VO^{2+}/VO_2^+$ reaction is slightly lower than that of the $Mn^{2+}/MnO_2$ reaction (1.01 V *vs.* 1.228 V), $VOSO_4$ is a suitable choice as a redox mediator for the $Mn^{2+}/MnO_2$ reaction. Through electrochemical measurements, *ex-situ* UV-visible (UV-vis) spectroscopy, X-ray diffraction (XRD), and scanning electron microscopes (SEM), we validate the interaction between $VO^{2+}$ and $MnO_2$, which effectively mitigates the accumulation of $MnO_2$. By employing this redox mediator, the $MnO_2/VOSO_4$-Zn battery exhibits exceptional redox reversibility and excellent cycling stability, even at high areal capacities. Specifically, it achieves 900 cycles at 5 mAh $cm^{-2}$ and 500 cycles at 10 mAh $cm^{-2}$. Notably, even in the flow battery device, the battery demonstrates stable cycling performance for over 300 cycles at 20 mAh $cm^{-2}$.

## EXPERIMENTAL

### Materials

Manganese sulfate monohydrate ($MnSO_4·H_2O$, 99%), zinc sulfate heptahydrate ($ZnSO_4·7H_2O$, 99%), and sodium sulfate ($Na_2SO_4$, 99%) were all received from Aladdin, Shanghai. Vanadium (IV) sulfate oxide hydrate ($VOSO_4·xH_2O$, 99.9%) was received from Macklin. Sulfuric acid ($H_2SO_4$, 99%) was sourced from the Guangzhou Chemical Reagent Factory. Carbon felt (5 mm in thickness) was purchased from CeTech Co. Ltd. Zinc foil (0.2 mm in thickness) was purchased from Tianjin Avixin Chemical Technology Co., Ltd. Cation exchange membrane Nafion 117 was acquired from Dupont.

### Cell assembly

In both static and flow batteries, carbon felts were applied as current collectors for the cathodes, and zinc foils were applied as the anodes. To prevent the shuttle effect of $VO^{2+}/VO_2^+$, the anode and cathode were separated by a cation exchange membrane (Nafion 117) in a battery. Anolytes consisted of 1 M $ZnSO_4$ and 0.5 M $H_2SO_4$. Catholytes of E-Mn (0.5 M $MnSO_4$ + 1 M $Na_2SO_4$ + 0.5 M $H_2SO_4$) and E-MnVO (0.5 M $MnSO_4$ + 0.05 M $VOSO_4$ + 1 M $Na_2SO_4$ + 0.5 M $H_2SO_4$) were used for the $MnO_2$-Zn and $MnO_2$/$VOSO_4$-Zn batteries, respectively. In a typical static battery, the anode and cathode were 1 cm × 1 cm in size. The anolyte and catholyte were both 5 mL. In the case of flow batteries, 25 mL of catholytes and anolytes were stored separately in two tanks. Electrolyte flow was driven by a peristaltic pump at a flow rate of approximately 40 mL $min^{-1}$.

### Material characterization

UV-vis spectra were acquired using a UV-VIS Spectrophotometer (Shimadzu, UV-2600). SEM was carried out using a TESCAN GAIA3 instrument. XRD analysis was performed utilizing a PANalytical Empyrean instrument with Cu Kα radiation. X-ray photoelectron spectroscopy (XPS) measurements were conducted using a Thermos Scientific K-Alpha instrument.

### Electrochemical measurements

In a typical three-electrode setup, the cathode employed carbon felt as a current collector, while a platinum plate served as the counter electrode, and a saturated calomel electrode (SCE) functioned as the reference electrode. Cyclic voltammetry (CV) and linear sweep voltammetry (LSV) were conducted using an electrochemical workstation (Gamry Interface1000). The CV was performed at a scanning rate of 0.5 mV $s^{-1}$, while the LSV was conducted at a scanning rate of 1 mV $s^{-1}$. Electrochemical impedance spectroscopy was performed on a Chenhua electrochemical workstation (CHI660e) across a frequency range of $10^5$-$10^{-2}$ Hz. Galvanostatic charge/discharge tests were carried out using a Neware battery analyzer. In these tests, the battery was charged up to a specific capacity and discharged until reaching a cutoff voltage of 1.0 V.

## RESULTS AND DISCUSSION

The electrochemical performance of the $Mn^{2+}/MnO_2$ was first studied using a three-electrode system. The electrolyte consisted of 0.5 M $MnSO_4$, 1 M $Na_2SO_4$, and 0.5 M $H_2SO_4$ (referred to as E-Mn). During the galvanostatic discharge/charge measurements [Figure 1A], E-Mn exhibits a cyclic life of less than 200 cycles when charged to 5 mAh and discharged to 0.2 V *vs.* SCE at an applied current density of 10 mA $cm^{-2}$. The limited cyclic life can be attributed to incomplete $MnO_2$ dissolution [Figure 2A]. As revealed in the SEM image [Supplementary Figure 1], a thick layer of $MnO_2$ remains on the carbon fiber after 30 cycles. Therefore, enhancing $MnO_2$ dissolution is imperative to extend the cyclic life of $Mn^{2+}/MnO_2$.

The electrolyte, denoted as E-VO, consists of 0.05 M $VOSO_4$, 1 M $Na_2SO_4$, and 0.5 M $H_2SO_4$. E-VO displays a pair of peaks at 0.75/0.71 V *vs.* SCE on the CV curve, corresponding to the redox reaction of $VO^{2+}/VO_2^+$ [Figure 1B]. When charged/discharged in the range of 0.2-1.1 V at a current density of 10 mA $cm^{-2}$, E-VO

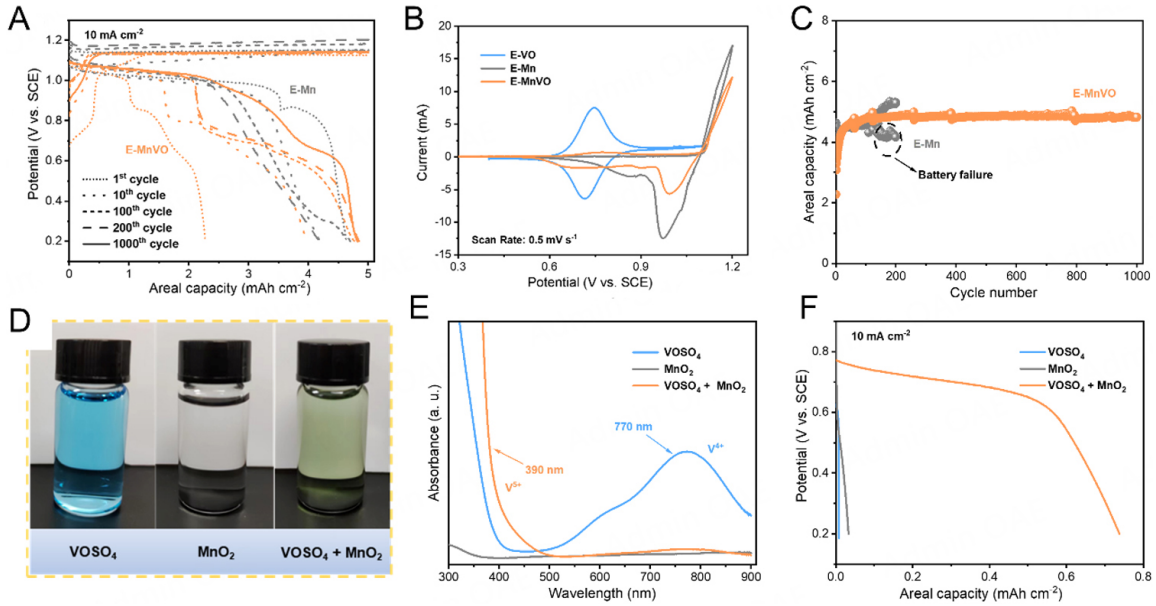


**Figure 1.** (A) Charge/discharge profiles, (B) CV curves of E-Mn, E-VO, and E-MnVO at 0.5 mV $s^{-1}$ and (C) cyclic performance of E-Mn and E-MnVO at 5 mAh $cm^{-2}$ and 10 mA $cm^{-2}$. (D) Optical images, (E) UV-vis spectra, and (F) discharge profiles of $VOSO_4$ solution, $MnO_2$ suspension, and a mixture of $VOSO_4$ and $MnO_2$.

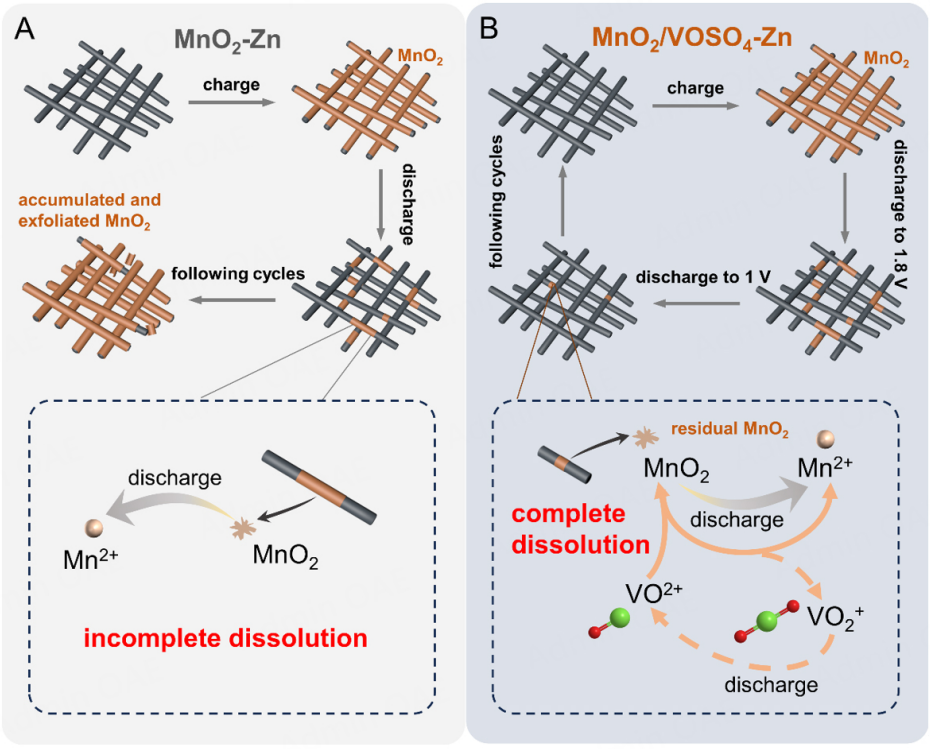


**Figure 2.** Schematic illustration of the charge/discharge process of the (A) $MnO_2$-Zn and (B) $MnO_2$/$VOSO_4$-Zn batteries.

exhibits a stable discharge capacity of ~0.42 mAh $cm^{-2}$ over 4,000 cycles [Supplementary Figure 2]. Comparatively, the $VO^{2+}/VO_2^+$ redox couple demonstrates a lower redox potential and improved cyclic

stability than $Mn^{2+}/MnO_2$, indicating that $VOSO_4$ is a suitable redox mediator for the conversion reaction of $Mn^{2+}/MnO_2$.

The cyclic performance of E-Mn at different $VOSO_4$ concentrations was evaluated [Supplementary Figure 3]. The E-Mn system with a $VOSO_4$ concentration of 0.02 M displays a relatively low coulombic efficiency and a short lifespan. While an addition of 0.1 M $VOSO_4$ improves the coulombic efficiency and cyclic stability, it results in a relatively low energy density. Consequently, a concentration of 0.05 M $VOSO_4$ was determined to be the optimal choice for the system, termed E-MnVO. The initial charge curve of E-MnVO exhibits a slope followed by a plateau at 1.13 V [Figure 1A], corresponding to the oxidation of $VO^{2+}$ prior to that of $Mn^{2+}$. The oxidation of $VO^{2+}$ contributes a capacity of ~0.5 mAh $cm^{-2}$, consistent with the charge capacity delivered by E-VO [Supplementary Figure 2]. Initially, E-MnVO displays low discharge capacities. After a few cycles of activation, the discharge capacity of E-MnVO gradually increases and stabilizes. This phenomenon may be attributed to the initial cycles where an excessive amount of $VO^{2+}$ ions cannot be fully oxidized into $VO_2^+$ ions during the charging process. These excess $VO^{2+}$ ions react with $MnO_2$, consequently depleting $MnO_2$, but without contributing to the discharge capacity. As a result, the discharge capacity is relatively lower during the initial cycles. However, after some cycles, the oxidation of $VO^{2+}$ ions contribute more capacity in the charge process as indicated by the lowered charge plateau, which may be because residual $MnO_2$ trap $Mn^{2+}$ ions in the electrolyte. The remaining $VO^{2+}$ ions are reduced in the electrolyte after the charge process, therefore leading to an increase of the discharge capacity. The discharge curve of the 100th cycle [Figure 1A] presents two plateaus, indicating the successive electrochemical reductions of $MnO_2$ (1.06 V) and $VO_2^+$ (0.69 V). This cycle delivers a capacity of 4.75 mAh $cm^{-2}$ with a coulombic efficiency of 95%. Moreover, the charge/discharge platforms of E-MnVO maintain stability throughout cycling, with a cyclic life exceeding 1,000 cycles [Figure 1A]. In contrast, the charge/discharge platforms of the E-Mn gradually increase over cycling, suggesting a decrease in pH value due to the accumulation of $MnO_2$. The capacity of E-Mn remains stable for only 200 cycles [Figure 1C]. SEM images [Supplementary Figure 4] demonstrate the accumulation of thick layers of $MnO_2$ on or exfoliating from the carbon fibers in E-Mn after 200 cycles. However, with the addition of $VOSO_4$, the accumulation of $MnO_2$ on the carbon felt significantly decreases after 200 cycles.

To elucidate the underlying mechanism of the $VOSO_4$ mediator, we conducted an experiment by adding $MnO_2$ powder into the blue $VOSO_4$ solution. As a result, the precipitate dissolved [Figure 1D], leading to a change in solution color to light yellow. Accordingly, the distinct peak on the UV-vis spectrum of $VOSO_4$, corresponding to $VO^{2+}$ (~770 nm)[37], disappeared upon the addition of $MnO_2$, suggesting a reaction between $VOSO_4$ and $MnO_2$ [Figure 1E]. Furthermore, we examined the discharge curves of the $VOSO_4$ solution, $MnO_2$ suspension, and a mixture of $VOSO_4$ and $MnO_2$. Individually, $VOSO_4$ and $MnO_2$ exhibited negligible capacities [Figure 1F], attributed to the reductive state of $VO^{2+}$ and the inadequate contact between $MnO_2$ suspended in the electrolyte and the carbon felt. However, when the mixture was formed, it became transparent and displayed a plateau at 0.70 V, indicating $MnO_2$ oxidizes $VO^{2+}$ to $VO_2^+$, which can subsequently undergo electrochemical reduction.

Therefore, the working principle of the $VOSO_4$ mediator to improve the dissolution of $MnO_2$ is depicted in Figure 2B. During the charging progress, the oxidation of $VO^{2+}$ precedes the deposition of $MnO_2$ on the carbon felt, generating $VO_2^+$ [Equation (3)]. Conversely, during discharge, $MnO_2$ dissolves into $Mn^{2+}$ prior to the reduction of $VO_2^+$. The reduction product $VO^{2+}$ then reacts with the residual $MnO_2$, leading to the formation of $VO_2^+$ and $Mn^{2+}$ [Equation (4)]. Moreover, the resulting $VO_2^+$ is subjected to another round of electrochemical reduction [Equation (3)], steadily providing a continuous supply of $VO^{2+}$ to react with $MnO_2$ until all the remaining $MnO_2$ is consumed. As a result, this process promotes the reversibility of the

$MnO_2$ deposition and dissolution.

$$VO^{2+} + H_2O \leftrightarrow VO_2^+ + 2H^+ + e^- \quad (3)$$

$$MnO_2 + 2VO^{2+} \rightarrow Mn^{2+} + 2VO_2^+ \quad (4)$$

To investigate the impact of the $VOSO_4$ mediator in the $MnO_2$-Zn full cell, we introduced $VOSO_4$ into the catholyte of a two-electrode configuration [Supplementary Figure 5]. First, we assessed the capacity contribution and stability of 0.05 M $VOSO_4$ in the $MnO_2$-Zn full cell. The $VOSO_4$-Zn batteries exhibit excellent cyclic stability, retaining a reversible capacity of 0.3 mAh $cm^{-2}$ even after 3,000 cycles [Supplementary Figure 6]. The $MnO_2$/$VOSO_4$-Zn battery, charged to 1 mAh $cm^{-2}$ at 10 mA $cm^{-2}$, exhibits stable charge/discharge performance for over 3000 cycles, surpassing the cyclic life of the $MnO_2$-Zn battery [Figure 3A and Supplementary Figure 7]. When the charging capacity increases to 5 mAh $cm^{-2}$, the $MnO_2$-Zn battery exhibits a high discharge plateau at 1.95 V and coulombic efficiency of 95% at 10 mA $cm^{-2}$ in the first cycle. However, after 150 cycles, the discharge plateau declines to 1.69 V, and the gap between the charge and discharge plateaus widens to 0.76 V [Figure 3B]. This decline in performance can be attributed to the accumulation of undissolved $MnO_2$, leading to serious polarization and high charge transfer resistance [Supplementary Figure 8], which results in a substantial loss in capacity. In comparison, the use of the $VOSO_4$ mediator reduces the discharge voltage. However, the $MnO_2$/$VOSO_4$-Zn battery demonstrates remarkable stability in charge/discharge cycles, exceeding 900 cycles and maintaining a high coulombic efficiency of approximately 98% [Figure 3C and D]. On the other hand, the energy efficiency of the $MnO_2$-Zn battery gradually declines over cycling, averaging around 60%. In contrast, the $MnO_2$/$VOSO_4$-Zn battery displays a stable energy efficiency of approximately 75% throughout cycling [Supplementary Figure 9].

Figure 3E and F compares the rate capability of the $MnO_2$-Zn battery and $MnO_2$/$VOSO_4$-Zn battery, ranging from 5 to 50 mA $cm^{-2}$. As a current density of 50 mA $cm^{-2}$, the $MnO_2$/$VOSO_4$-Zn battery exhibits a discharge plateau at 1.77 V, maintaining a reversible capacity of 3.50 mAh $cm^{-2}$ and an energy density of 5.42 mWh $cm^{-2}$. In contrast, the $MnO_2$-Zn cell displays a lower discharge voltage of 1.67 V, with a reversible capacity of 3.09 mAh and an energy density of 4.63 mWh $cm^{-2}$. Additionally, even when charged to 10 mAh $cm^{-2}$ at 1 C [Figure 3G], the $MnO_2$/$VOSO_4$-Zn battery exhibits a high coulombic efficiency of 97 % and an energy efficiency of 79% after 500 cycles [Supplementary Figure 10]. On the other hand, the $MnO_2$-Zn battery fails to deliver capacity after 100 cycles. These comparisons of the charge/discharge performance clearly highlight the effectiveness of $VOSO_4$ as a mediator in enhancing the cyclic stability of the $MnO_2$-Zn battery.

To investigate the influence of $VOSO_4$ on the deposition and dissolution behavior of $Mn^{2+}$, extensive characterization was performed on the cathodes of the $MnO_2$/$VOSO_4$-Zn and $MnO_2$-Zn batteries using XRD, SEM, and XPS after charge and discharge cycles. Following the 20th charging at 5 mAh $cm^{-2}$ and 10 mA $cm^{-2}$, diffraction peaks corresponding to ε-$MnO_2$ (JCPDS #30-0820) can be observed in the XRD pattern of the cathode from the $MnO_2$/$VOSO_4$-Zn battery [Figure 4A]. The broad peaks with low intensity indicate low crystallinity of the deposited ε-$MnO_2$. SEM images [Figure 4B and C] reveal a dense layer of $MnO_2$ layer composed of nanoparticles. XPS analysis of the charged cathode shows peaks at 84.16 and 89.26 eV in the Mn 3s region, corresponding to $Mn^{4+}$ [Figure 4D]. Peaks at 529.9 and 531.3 eV in the O1s region correspond to the Mn-O-Mn and Mn-OH bonds, respectively [Figure 4E][12]. Notably, the energy splitting of $Mn^{4+}$ peaks in the charged cathode of the $MnO_2$/$VOSO_4$-Zn battery is higher than that in the $MnO_2$-Zn battery (5.10 eV *vs.* 4.99 eV) [Supplementary Figure 11], suggesting the formation of lower-

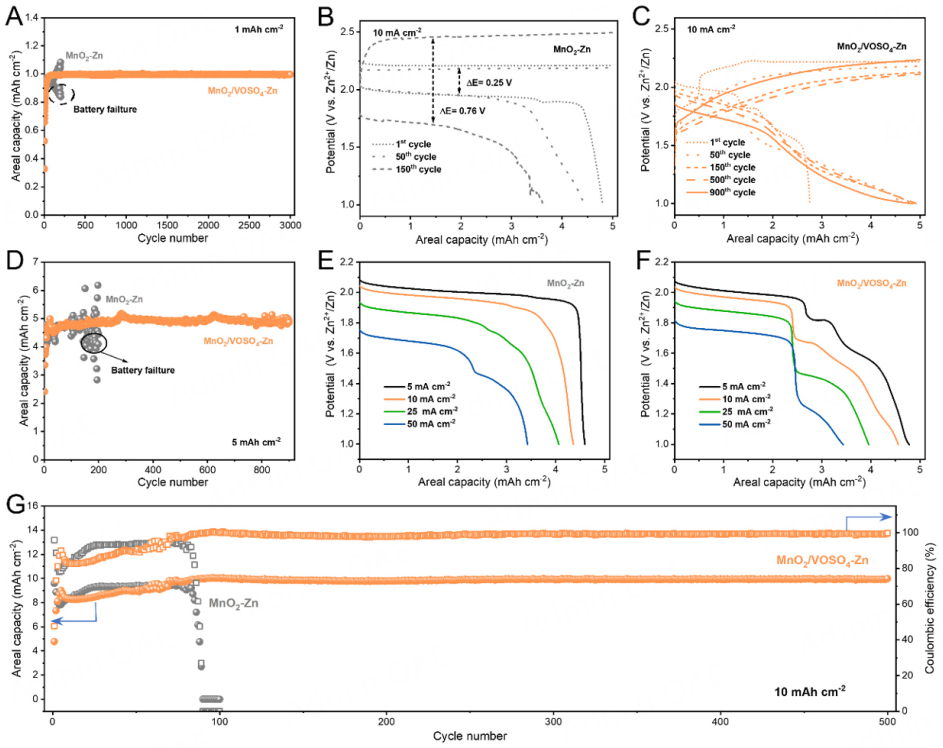


**Figure 3.** Electrochemical performance of the $MnO_2$-Zn and $MnO_2$/$VOSO_4$-Zn batteries: (A) Cycling performance at 1 mAh $cm^{-2}$, (B and C) charge and discharge curves, and (D) cyclic performance at 5 mAh $cm^{-2}$ and 10 mA $cm^{-2}$,(E and F) discharge curves at 5 mAh $cm^{-2}$ and various current densities, and (G) cyclic performance at 10 mAh $cm^{-2}$ and 10 mA $cm^{-2}$.

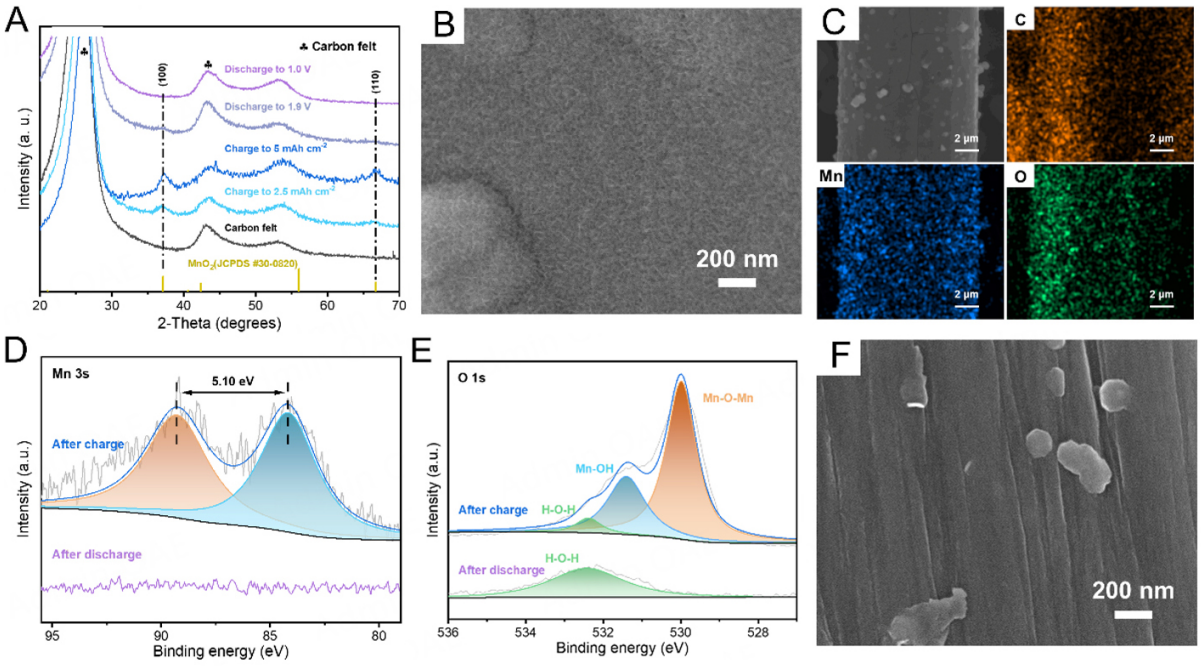


**Figure 4.** Characterizations of the cathode in the $MnO_2$/$VOSO_4$-Zn battery in the 20th cycle: (A) XRD patterns at different states, (B) SEM and (C) EDS elemental mapping images after charge, (F) SEM image after discharge, XPS spectra in the region of (D) Mn 3s and (E) O 1s.

valence Mn during the deposition[33,39]. The $VOSO_4$ mediator introduces more defects in $MnO_2$, thereby promoting its dissolution. After subsequent discharge to 1.0 V, the peaks corresponding to ε-$MnO_2$ disappear in the XRD pattern [Figure 4A], and the surface of the carbon fiber appears bare and smooth in the SEM image [Figure 4F, Supplementary Figure 12]. Additionally, the peaks associated with $Mn^{4+}$, Mn-O-Mn, and Mn-OH disappear in the XPS spectrum, indicating good reversibility of $MnO_2$ deposition and dissolution. After 100 cycles, the ε-phase $MnO_2$ peaks are nearly absent in the XRD pattern of the cathode [Figure 5A], and only a few residual $MnO_2$ particles are observed in the SEM image [Figure 5B and C]. These SEM and XRD measurements conclusively confirmed that $MnO_2$ can be completely dissolved by the $VOSO_4$ mediator during cycling.

Regarding the cathode of the $MnO_2$-Zn battery, the XRD pattern consistently exhibits increasingly intense diffraction peaks corresponding to $MnO_2$ after 20 cycles [Supplementary Figure 13] and 100 cycles [Figure 5D]. SEM images reveal a remaining $MnO_2$ layer on the carbon fiber with a thickness of approximately 6 μm after 20 cycles [Supplementary Figures 14 and 15], which further grows to 14 μm after 100 cycles [Figure 5E and F]. Furthermore, some $MnO_2$ particles even detach from the carbon felt, obstructing ion transport channels on the membrane [Figure 6A]. The accumulation and detachment of $MnO_2$ ultimately lead to the failure of the $MnO_2$-Zn battery.

Figure 6A provides a comparison of the Nafion membranes from the $MnO_2$/$VOSO_4$-Zn and $MnO_2$-Zn batteries after 100 cycles. The membrane in the $MnO_2$/$VOSO_4$-Zn battery remains transparent, while the membrane in the $MnO_2$-Zn battery turns black due to the migration of $MnO_2$. However, the blackened membrane regains transparency after immersion in E-MnVO. The $MnO_2$-Zn battery experienced failure after 218 cycles. When $VOSO_4$ is added to the catholyte of the failed $MnO_2$-Zn battery, the battery exhibits a discharge capacity of 31 mAh $cm^{-2}$. Because a significant amount of $MnO_2$ accumulated on the carbon felt or suspended within the catholyte reacts with $VO^{2+}$ ions, generating $VO_2^+$ ions, which contribute discharge capacity through the electrochemical reduction. After $VOSO_4$ completely transforms the accumulated $MnO_2$ into $Mn^{2+}$, the battery is successfully revived and demonstrates stable charge/discharge behavior in subsequent cycles [Figure 6B and C]. Conversely, replacing the zinc foil in the failed $MnO_2$-Zn battery does not resolve the abnormal charge/discharge performance [Supplementary Figure 16]. This comparison indicates that the failure of the $MnO_2$-Zn battery is primarily attributed to the accumulation of undissolved $MnO_2$ rather than the degradation of the zinc anode. Hence, the use of the $VOSO_4$ mediator proves effective in extending the lifespan of the $MnO_2$-Zn battery.

Additionally, we introduced the $VOSO_4$ mediator into the catholyte of the $MnO_2$-Zn flow battery [Supplementary Figure 17], resulting in the achievement of even higher area capacity. As depicted in Figure 6D and E, when the charge capacity is increased to 20 mAh $cm^{-2}$, the flow battery exhibits stable cyclic performance with a coulombic efficiency of approximately 97% and an energy density of 30.32 mWh $cm^{-2}$ after 300 cycles. Remarkably, even at 30 mAh $cm^{-2}$, the flow battery achieves 90 stable cycles with excellent reversibility [Supplementary Figure 18]. Furthermore, the summarized results in Figure 6F and Supplementary Table 1 illustrate that our assembled $MnO_2$/$VOSO_4$-Zn battery displays outstanding performance in terms of areal capacity, reversibility, and cycle life compared with the reported electrolytic $MnO_2$-based batteries. To upscale the battery, a carbon felt measuring 64 $cm^2$ (8 cm × 8 cm) was utilized as the current collector for the cathode, resulting in the assembly of a larger-scale $MnO_2$/$VOSO_4$-Zn battery with a charge capacity of 600 mAh [Supplementary Figure 19]. This battery demonstrates good cyclic stability, maintaining approximately 500 mAh and 751 mWh over 20 cycles, highlighting the potential of the $MnO_2$/$VOSO_4$-Zn battery for practical energy storage applications.

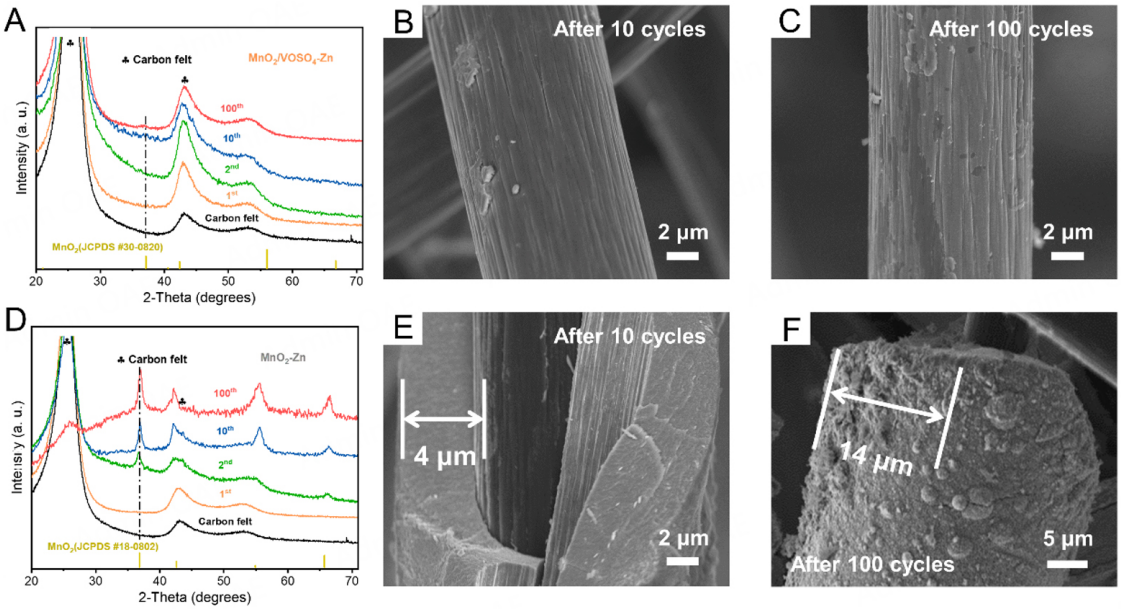


**Figure 5.** Comparisons of the cathodes in the $MnO_2$/$VOSO_4$-Zn and $MnO_2$-Zn batteries after cycling: (A) XRD patterns, SEM images after (B) 10 and (C) 100 cycles of the cathode in the $MnO_2$/$VOSO_4$-Zn battery. (D) XRD patterns, SEM images after (E) 10 and (F) 100 cycles of the cathodes in the $MnO_2$-Zn battery.

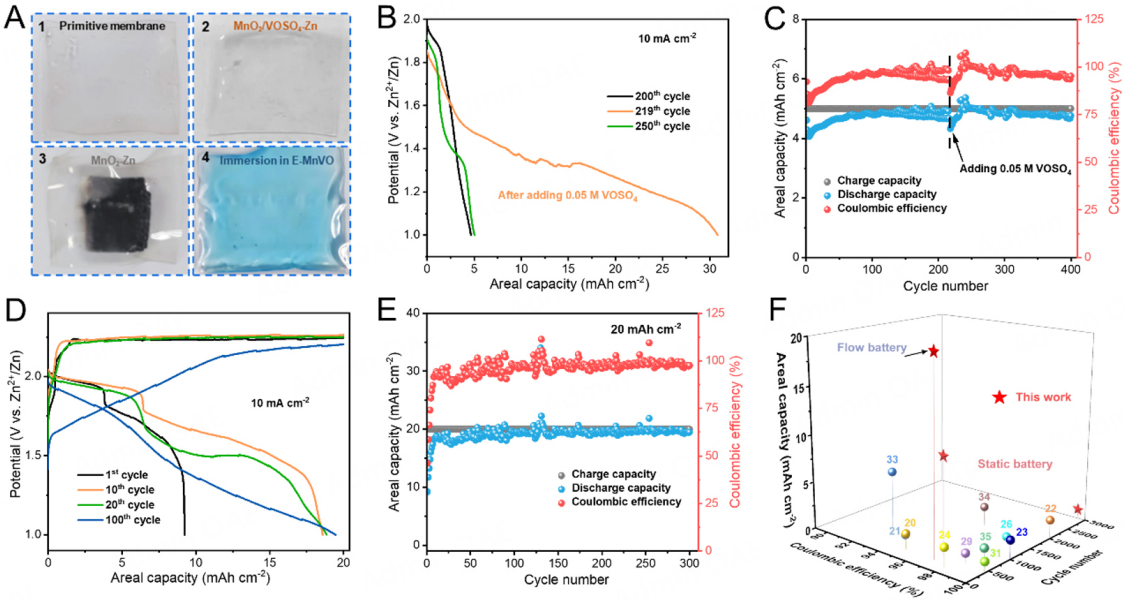


**Figure 6.** (A) Comparisons of Nafion membranes obtained from the cycled $MnO_2$/$VOSO_4$-Zn and $MnO_2$-Zn batteries before and after immersion in E-MnVO. (B) Discharge curves and (C) cyclic performance of the failed $MnO_2$-Zn battery after addition of $VOSO_4$ at 5 mAh $cm^{-2}$ and 10 mA $cm^{-2}$. (D) Charge/discharge curves and (E) cyclic performance of $MnO_2$/$VOSO_4$-Zn flow battery at 20 mAh $cm^{-2}$ and 10 mA $cm^{-2}$. (F) Comparison of the electrochemical performance of reported electrolytic $MnO_2$-based batteries.

## CONCLUSIONS

In conclusion, our study demonstrates significant improvements in the reversibility and cycling stability of $MnO_2$-Zn batteries through the utilization of redox mediator $VOSO_4$. The oxidation reaction involving $VO^{2+}$ effectively interacts with residual $MnO_2$, facilitating its dissolution. As a result, when this mediator

strategy is adopted in the $MnO_2$-Zn battery, it exhibits an impressive long cycle life of 500 cycles, even at a high area capacity of 10 mAh $cm^{-2}$, while maintaining a coulombic efficiency of approximately 97%. Furthermore, the $MnO_2$/$VOSO_4$-Zn flow battery demonstrates excellent cycle stability, maintaining performance over 300 cycles at 20 mAh $cm^{-2}$. These findings provide valuable insights into the potential large-scale application of electrolytic $MnO_2$-Zn batteries.

## DECLARATIONS

### Authors' contributions

Investigation, data curation, writing - original draft: Xu Y
Formal analysis: Huang W, Liu J, Hu R, Ouyang L
Resources, supervision, writing - review & editing, project administration: Yang L
Resources, project administration: Zhu M

### Availability of data and materials

The data supporting our findings can be found in the Supplementary Material.

### Financial support and sponsorship

We thank the financial support from the National Key Research and Development Program of China (2022YFB2502003) and the Guangdong Basic and Applied Basic Research Foundation (2023B1515040011).

### Conflicts of interest

All authors declared that there are no conflicts of interest.

### Ethical approval and consent to participate

Not applicable.

### Consent for publication

Not applicable.



## REFERENCES

1. Goodenough JB, Park KS. The Li-ion rechargeable battery: a perspective. *J Am Chem Soc* 2013;135:1167-76. DOI PubMed
2. Duffner F, Kronemeyer N, Tübke J, Leker J, Winter M, Schmuch R. Post-lithium-ion battery cell production and its compatibility with lithium-ion cell production infrastructure. *Nat Energy* 2021;6:123-34. DOI
3. He W, Guo W, Wu H, et al. Challenges and recent advances in high capacity Li-rich cathode materials for high energy density lithium-ion batteries. *Adv Mater* 2021;33:e2005937. DOI
4. Goodenough JB, Kim Y. Challenges for rechargeable Li batteries. *Chem Mater* 2010;22:587-603. DOI
5. Wang X, Zhang Z, Xi B, et al. Advances and perspectives of cathode storage chemistry in aqueous zinc-ion batteries. *ACS Nano* 2021;15:9244-72. DOI
6. Zeng X, Hao J, Wang Z, Mao J, Guo Z. Recent progress and perspectives on aqueous Zn-based rechargeable batteries with mild aqueous electrolytes. *Energy Stor Mater* 2019;20:410-37. DOI
7. Jia X, Liu C, Neale ZG, Yang J, Cao G. Active materials for aqueous zinc ion batteries: synthesis, crystal structure, morphology, and electrochemistry. *Chem Rev* 2020;120:7795-866. DOI
8. Kim S, Shan X, Abeykoon M, Kwon G, Olds D, Teng X. High-capacity aqueous storage in vanadate cathodes promoted by the Zn-ion and proton intercalation and conversion-intercalation of vanadyl ions. *ACS Appl Mater Interfaces* 2021;13:25993-6000. DOI PubMed
9. Zheng X, Ahmad T, Chen W. Challenges and strategies on Zn electrodeposition for stable Zn-ion batteries. *Energy Stor Mater* 2021;39:365-94. DOI
10. Zhao Q, Huang X, Zhou M, et al. Proton Insertion promoted a polyfurfural/$MnO_2$ nanocomposite cathode for a rechargeable aqueous Zn-$MnO_2$ battery. *ACS Appl Mater Interfaces* 2020;12:36072-81. DOI

11. Li L, Hoang TKA, Zhi J, Han M, Li S, Chen P. Correction to "functioning mechanism of the secondary aqueous Zn-β-$MnO_2$ battery". *ACS Appl Mater Interfaces* 2021;13:36653. DOI
12. Chen W, Li G, Pei A, et al. A manganese-hydrogen battery with potential for grid-scale energy storage. *Nat Energy* 2018;3:428-35. DOI
13. Wang M, Zheng X, Zhang X, et al. Opportunities of aqueous manganese-based batteries with deposition and stripping chemistry. *Adv Energy Mater* 2021;11:2002904. DOI
14. Liang G, Mo F, Li H, et al. A universal principle to design reversible aqueous batteries based on deposition-dissolution mechanism. *Adv Energy Mater* 2019;9:1901838. DOI
15. Zhang C. Made cheaper with sulfur and manganese. *Nat Energy* 2023;8:6. DOI
16. Chen N, Wang W, Ma Y, et al. Aqueous zinc-chlorine battery modulated by a $MnO_2$ redox adsorbent. *Small Methods* 2023:e2201553. DOI
17. Wang M, Chen N, Zhu Z, et al. Electrode-less $MnO_2$-metal batteries with deposition and stripping chemistry. *Small* 2021;17:e2103921. DOI
18. Yu Y, Zhang H, Yang F, Zeng Y, Liu X, Lu X. Bismuth nanoparticles@carbon composite as a stable and high capacity anode for high-voltage bismuth-manganese batteries. *Energy Stor Mater* 2021;41:623-30. DOI
19. Chao D, Zhou W, Ye C, et al. An electrolytic Zn-$MnO_2$ Battery for high-voltage and scalable energy storage. *Angew Chem Int Ed* 2019;58:7823-8. DOI
20. Yu X, Song Y, Tang A. Tailoring manganese coordination environment for a highly reversible zinc-manganese flow battery. *J Power Sources* 2021;507:230295. DOI
21. Xu Q, Xie Q, Xue T, et al. Salt bridge-intermediated three phase decoupling electrolytes for high voltage electrolytic aqueous Zinc-Manganese dioxides battery. *Chem Eng J* 2023;451:138775. DOI
22. Gou L, Li J, Liang K, Zhao S, Li D, Fan X. Bi-MOF modulating $MnO_2$ deposition enables ultra-stable cathode-free aqueous zinc-ion batteries. *Small* 2023;19:e2208233. DOI
23. Liu Y, Nan M, Zhao Z, et al. Manganese-based flow battery based on the $MnCl_2$ electrolyte for energy storage. *Chem Eng J* 2023;465:142602. DOI
24. Zeng X, Liu J, Mao J, et al. Toward a reversible $Mn^{4+}/Mn^{2+}$ redox reaction and dendrite-free Zn anode in near-neutral aqueous Zn/$MnO_2$ Batteries via salt anion chemistry. *Adv Energy Mater* 2020;10:1904163. DOI
25. Zhong C, Liu B, Ding J, et al. Decoupling electrolytes towards stable and high-energy rechargeable aqueous zinc-manganese dioxide batteries. *Nat Energy* 2020;5:440-9. DOI
26. Li G, Chen W, Zhang H, et al. Membrane-free Zn/$MnO_2$ flow battery for large-scale energy storage. *Adv Energy Mater* 2020;10:1902085. DOI
27. Liu Z, Yang Y, Lu B, Liang S, Fan HJ, Zhou J. Insights into complexing effects in acetate-based Zn-$MnO_2$ batteries and performance enhancement by all-round strategies. *Energy Stor Mater* 2022;52:104-10. DOI
28. Xiao X, Zhang Z, Wu Y, et al. Ultrahigh-loading manganese-based electrodes for aqueous batteries via polymorph tuning. *Adv Mater* 2023;35:e2211555. DOI
29. Liu C, Chi X, Han Q, Liu Y. A high energy density aqueous battery achieved by dual dissolution/deposition reactions separated in acid-alkaline electrolyte. *Adv Energy Mater* 2020;10:1903589. DOI
30. Lei J, Yao Y, Wang Z, Lu Y. Towards high-areal-capacity aqueous zinc-manganese batteries: promoting $MnO_2$ dissolution by redox mediators. *Energy Environ Sci* 2021;14:4418-26. DOI
31. Chao D, Ye C, Xie F, et al. Atomic engineering catalyzed $MnO_2$ electrolysis kinetics for a hybrid aqueous battery with high power and energy density. *Adv Mater* 2020;32:e2001894. DOI PubMed
32. Yadav GG, Gallaway JW, Turney DE, et al. Regenerable Cu-intercalated $MnO_2$ layered cathode for highly cyclable energy dense batteries. *Nat Commun* 2017;8:14424. DOI PubMed PMC
33. Zheng X, Wang Y, Xu Y, et al. Boosting electrolytic $MnO_2$-Zn Batteries by a bromine mediator. *Nano Lett* 2021;21:8863-71. DOI
34. Shen X, Wang X, Zhou Y, et al. Highly reversible aqueous Zn-$MnO_2$ battery by supplementing $Mn^{2+}$-mediated $MnO_2$ deposition and dissolution. *Adv Funct Mater* 2021;31:2101579. DOI
35. Chuai M, Yang J, Tan R, et al. Theory-driven design of a cationic accelerator for high-performance electrolytic $MnO_2$-Zn batteries. *Adv Mater* 2022;34:e2203249. DOI
36. Qin Z, Song Y, Yang D, et al. Enabling reversible $MnO_2/Mn^{2+}$ transformation by $Al^{3+}$ addition for aqueous Zn-$MnO_2$ hybrid batteries. *ACS Appl Mater Interfaces* 2022;14:10526-34. DOI
37. Choi C, Kim S, Kim R, et al. A review of vanadium electrolytes for vanadium redox flow batteries. *Renew Sustain Energy Rev* 2017;69:263-74. DOI
38. Liu Y, Shen Y, Yu L, et al. Holey-engineered electrodes for advanced vanadium flow batteries. *Nano Energy* 2018;43:55-62. DOI
39. Sun M, Lan B, Lin T, et al. Controlled synthesis of nanostructured manganese oxide: crystalline evolution and catalytic activities. *CrystEngComm* 2013;15:7010-18. DOI